PHYSICAL REVIEW B **94**, 064520 (2016)

Tuning Yu-Shiba-Rusinov states in a quantum dot

Anders Jellinggaard, Kasper Grove-Rasmussen,* Morten Hannibal Madsen, and Jesper Nygård
Center for Quantum Devices, Niels Bohr Institute, University of Copenhagen, Universitetsparken 5, 2100 Copenhagen, Denmark
(Received 19 April 2016; revised manuscript received 20 July 2016; published 29 August 2016)

We present transport spectroscopy of subgap states in a bottom gated InAs nanowire coupled to a normal lead and a superconducting aluminium lead. The device shows clearly resolved subgap states which we can track as the coupling parameters of the system are tuned and as the gap is closed by means of a magnetic field. We systematically extract system parameters by using numerical renormalization-group theory fits as a level of the quantum dot is tuned through a quantum phase transition electrostatically and magnetically. We also give an intuitive description of subgap excitations.

DOI: 10.1103/PhysRevB.94.064520

I. INTRODUCTION

Hybrid superconductor-quantum dot devices [1] are heavily employed in recent experimental programs. For instance, quantum dots serve as an integral component of proposals to form [2,3], manipulate [4–6], and probe [7–9] Majorana bound states [10,11]. In Cooper pair splitters, the dynamics of quantum dots filter local Andreev reflections from the desired nonlocal Andreev reflections to form a source of entangled electrons [12–14].

In a dot-superconductor system, where the charging energy is larger than the order parameter, quasiparticles in the superconductor bind to the dot by the exchange interaction and give rise to subgap excitations [15]. When these quasiparticles form a singlet with electrons on the dot, the resultant states are called Yu-Shiba-Rusinov states [16–18] and have historically been investigated primarily through scanning tunneling microscopy [19,20]. Only recently have these excitations been observed in transport experiments [21–33]. We will give an intuitive description of subgap excitations in the following section.

To experimentally investigate subgap excitations, we fabricated a bottom gated normal-metal/nanowire/superconductor device (N-NW-S), which allows for the formation of a gate defined quantum dot proximitized to the superconductor. The device shows clearly resolved subgap states that we can track as the device is electrostatically tuned. In this way we follow a single charge state of the dot, through the doublet to singlet quantum phase transitions occurring as the barrier to the superconductor is lowered. We fit measured excitations energies to a simulation developed for this purpose using the nonperturbative numerical renormalization-group (NRG) method [32,34,35], and in this way systematically extract physical parameters of the device.

The system investigated is in many ways similar to N-NW-S devices where Majorana bound states have been examined [36–38], and a good understanding of the magnetic field behavior of proximitized nanowire quantum dots is necessary to understand transport data of these similar devices. We probe in detail the magnetic field behavior and observe excitations apparently clinging to zero bias as the gap is about to close, consistent with a recent experiment [21].

A. Subgap states

We consider a quantum dot described by the Anderson model (full Hamiltonian in Appendix B) with a single level at ϵ and a charging energy of U, coupled to a normal lead and to a superconducing lead with order parameter Δ. The strength of the coupling to lead α ($\alpha = N,S$), is governed by the corresponding tunneling density of states, $\Gamma_\alpha = 2\pi|t_\alpha|^2\nu_F$, where t_α is the tunneling coefficient of lead α and ν_F is the density of states of lead α near the Fermi level. Our data are collected in a regime where Γ_N is small compared to the other energies of the system, so we consider the normal lead to be a tunnel probe[1] which is used to probe the quantum dot/superconductor system.

The nature of subgap excitations in such a system depends on the relative size of Δ and U [15]. If Δ is large, the system can be understood in terms of repeated Andreev reflections giving rise to Andreev bound states [40]. When U is large, Andreev reflections are suppressed, and instead we need to think in terms of quasiparticles (Bogoliubons) in the superconducting lead. We will here develop an intuition for excitations in this case.

First, for vanishing Γ_S, we know exactly what the eigenstates of the model are, and we will be focusing, in particular, on the states shown in Fig. 1. These are the lowest energy singlets and doublets (only half the doublets are shown) for different values of ϵ. The illustrated states are

$$|A\rangle = |0\rangle, \qquad |D\rangle = \gamma_\uparrow^\dagger|0\rangle,$$
$$|B\rangle = \frac{1}{\sqrt{2}}(\gamma_\downarrow^\dagger d_\uparrow^\dagger - \gamma_\uparrow^\dagger d_\downarrow^\dagger)|0\rangle, \qquad |E\rangle = d_\uparrow^\dagger|0\rangle,$$
$$|C\rangle = d_\uparrow^\dagger d_\downarrow^\dagger|0\rangle, \qquad |F\rangle = d_\uparrow^\dagger d_\downarrow^\dagger \gamma_\uparrow^\dagger|0\rangle,$$

where we have defined $\gamma_\sigma^\dagger$ as the operator that creates the lowest energy Bogoliubon [41] with spin σ, and $d_\sigma^\dagger$ as the operator which creates an electron on the dot with spin σ. The figure also shows the energy of relevant excitations between these states.

As Γ_S is turned up, the singlet states are mixed resulting in avoided crossings, and the same happens for the different

*Corresponding author: k_grove@fys.ku.dk

[1]Recent numerical work suggests that the normal lead may have a nonpertubative effect on the system, so this approximation may not be entirely justified [39].

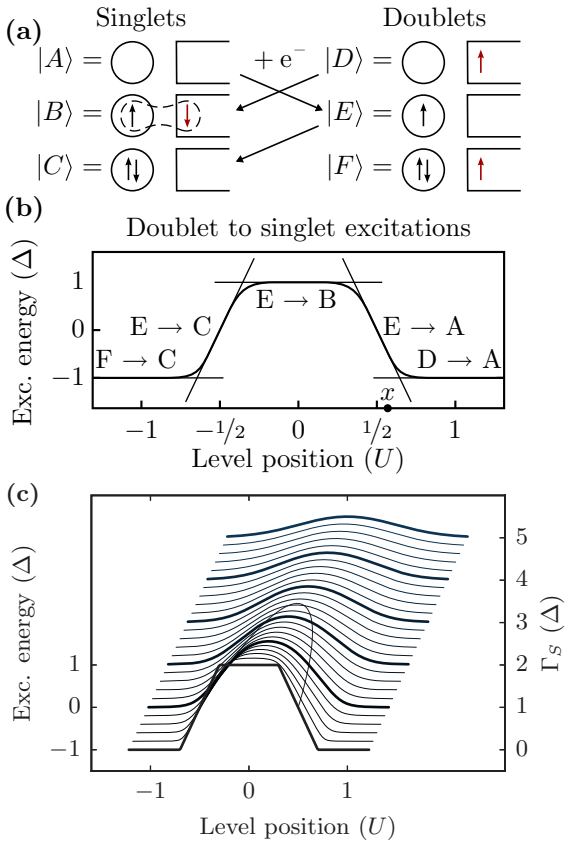

FIG. 1. Excitations between states in a quantum dot/superconductor system. (a) The states under consideration with arrows in circles representing electrons in the dot and arrows in open rectangles representing Bogoliubons. The dashed shape in the diagram for $|B\rangle$ depicts a singlet correlation. The arrows annotated with $+e^-$ show dominant sequential tunneling processes for transport going from N to S at the level position marked x in (b). (b) A schematic diagram showing subgap excitations in the system, with and without anticrossings induced by the coupling between the dot and superconductor. (c) NRG simulations of the lowest doublet to singlet transitions for different values of the coupling density of states, Γ_S. For all curves in (c), we have $U = 5\Delta$. The curve going across the traces mark an excitation energy of zero. Traces have been offset for clarity as indicated on the right-hand axis.

doublet states. For instance, the coupling between $|A\rangle$ and $|B\rangle$ causes the excitation energy inside the gap to move down towards the center of the gap. The other Bogoliubons (those of higher energy) will all move the subgap excitation in the same direction.

Eventually, this simple picture breaks down, as states with more than one Bogoliubon become a significant factor in forming the low-energy eigenstates. For higher Γ_S, it is not possible to find a simple theory that covers the entire range of ϵ and lends itself to a clear physical understanding, and one has to resort to numerical procedures. In this vein, Fig. 1(c) shows the lowest energy doublet to singlet excitation as a function of the level position and Γ_S as found using NRG simulations. In the middle of the Coulomb valley the doublet to singlet excitation energy decreases with increasing Γ_S, indicating a stabilization of the singlet state, and eventually the energy crosses zero, which is an example of a second-order quantum phase transition [21,42]. For larger Γ_S, the ground state remains a singlet for all level positions, even as the expected number of electrons on the dot changes by 2.

The NRG method has been applied to the proximitized Kondo model [43,44], the proximitized Anderson model [45], and to the normal-metal/quantum dot/superconductor system [39,46] in the literature, and generally recreates the features seen in real systems fairly accurately, as our fits below also indicate. Note, that we are using a newly written implementation of the NRG program which does not exploit symmetries in the system to speed up the algorithm [47]. Consequently, we only keep 160 states from each link of the chain. In Appendix C we compare results from our program to the phase diagram in Ref. [39] to show that there is reasonable agreement between the output from our program and that of an established program running a simulation with more states retained.

B. Transport

We imagine that transport in the device is primarily sequential in electrons tunneling from the N electrode to the dot-S system. This is possible once states with different numbers of fermions are mixed. In Fig. 1(a) we have tried to illustrate the dominant sequential transport processes moving electrons from N to S when the level position is near $\frac{1}{2}U$, i.e., at x in Fig. 1(b). In this case, considering again—artificially—only one Bogoliubon state, the lowest energy singlet $|s\rangle$ is a linear combination of primarily $|A\rangle$ but with some weight on $|B\rangle$ and $|C\rangle$, and the lowest energy doublet $|d\rangle$ consists mainly of $|E\rangle$ with some weight on $|D\rangle$ and $|F\rangle$. Transport occurs by repeatedly swapping the state between $|s\rangle$ and $|d\rangle$ by adding electrons to the dot from the N lead.

Fermi's "golden rule" tells us that the rate at which we go from $|s\rangle$ to $|d\rangle$ is proportional to $|\langle d|d^\dagger_\uparrow|s\rangle|^2$ which, for low Γ_S, is close to what we would expect for a nonproximitized dot. Going from $|d\rangle$ to $|s\rangle$ occurs at a rate proportional to $|\langle s|d^\dagger_\uparrow|d\rangle|^2$, which is smaller because only terms involving $|B\rangle$ and $|D\rangle$ or $|C\rangle$ contribute, cf. Fig. 1(a). Intuitively, we have to move two electrons across the barrier to S in this transport process.

II. EXPERIMENTAL RESULTS

The device is a bottom gated 70-nm-diameter InAs nanowire with one Ti/Au contact and one Ti/Al contact approximately 330 nm apart. The bottom gates have a 55-nm center-to-center distance and are separated from the nanowire by a 24-nm HfO_2 dielectric. The contacts are both well coupled to the nanowire compared to the deliberate transport barriers we impose with the bottom gates to form the dot, and the Ti/Al contact is superconducting with $\Delta = 0.14$ mV. Further fabrication details can be found in Appendix A. Figure 2(a) shows a scale model of our device and our designation of a "tuning gate," V_T, and a "plunger gate," V_P. A scanning electron microscopy (SEM) micrograph of a similar device is shown in Fig. 2(b), where only the nanowire segment between the N and S electrodes is probed by transport. In all plots, we apply a bias V_{sd} to the aluminium contact and measure differential conductance dI/dV through the device

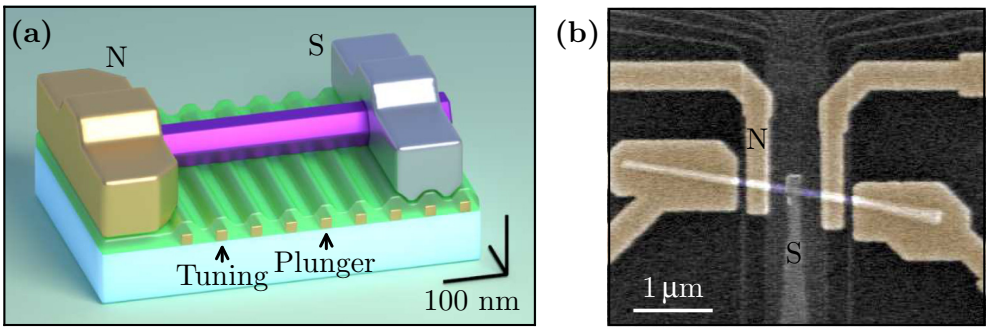

FIG. 2. (a) Artist impression of a 0.6-μm × 0.4-μm cutout of the device, to scale. The model shows the surface of the SiO_2 substrate, bottom gates, insulating HfO_2 (shown in green), InAs nanowire, gold contact, and aluminium contact. Details are in Appendix A. We assign names to two of the gates as shown. (b) SEM micrograph of a lithographically similar device. Note that only the part of the device between the gold electrode, N, and the aluminium electrode, S, is used.

at a temperature of 35 mK. Figure 3(a) shows typical transport data with the aluminium contact driven normal by a field, and Fig. 3(b) shows corresponding bias spectroscopy at zero field where the superconducting gap is visible as a horizontal band of low differential conductance between $V_{sd} = -0.14$ and 0.14 mV. The normal-state data show the usual Coulomb diamonds for $V_P < 1.6$ V, but for $V_P > 1.6$ V these diamonds become difficult to resolve, as the excitations are heavily tunnel broadened by the coupling of the aluminium contact. In regions where the excitations are broadened in the normal-state data [cf. Fig. 3(a)], which we attribute to a strong coupling to the aluminium contact, we see that the subgap excitations in Fig. 3(b) are pushed far inside the gap. In the remainder of this paper, we investigate how these subgap excitations respond to gate tuning and to small (less than B_c) magnetic fields.

A. Gate tuning

Figure 4 shows the zero-bias differential conductance of the device as a function of the potential, V_P and V_T, of the plunger and tuning gate. Both gates couple to the dot and have capacitances of $C_P \approx 5.5$ aF and $C_T \approx 3$ aF (lever arms $\alpha_P \approx 0.035$ and $\alpha_T \approx 0.02$) for the plunger and tuning gates, respectively. We define $V_P' = V_P + (V_T - 0.3\,\mathrm{V}) \times 0.57$ to compensate for this cross capacitance, and will use this for all subsequent figures instead of V_P. Note the overall increase in conductance for increasing V_T, which we ascribe to a lowering of the barrier to the normal lead consistent with the position of the tuning gate. Later, we shall see that Γ_N depends on V_T exponentially, which supports this assertion. Also evident in these plots is a quantum phase transition (at the *), which will become clearer in later plots.

Figure 5 shows how the subgap excitations respond to tuning, and a few trends are apparent going from low (a_0) to high (a_6) V_T. First, we see again the overall increase in conductance with higher V_T. Second, as V_T is changed, the subgap excitations of Fig. 5 shift in energy, with no overall trend, which we interpret as mesoscopic fluctuations of Γ_S as the wave functions of the dot states are perturbed by the changing V_T and V_P. The quantum phase transition is very clear in this plot, occurring for the charge state labeled IV around $V_T = 0.44$ V, i.e., between a_3 and a_4. The other charge states do not undergo this kind of quantum phase transition in the data shown. We point out that the transitions are not significantly tunnel broadened compared to the size of the gap, so we can assume that normal lead is weakly coupled to the dot.

To extract quantitative parameters for the system, we fit a model to the data consisting of single levels independently interacting with the superconductor, such that each level is described by the proximitized Anderson model. In this model, each level is described by the following parameters: the charging energy U, the potential of the plunger gate at the center of the corresponding Coulomb valley V_0, the plunger

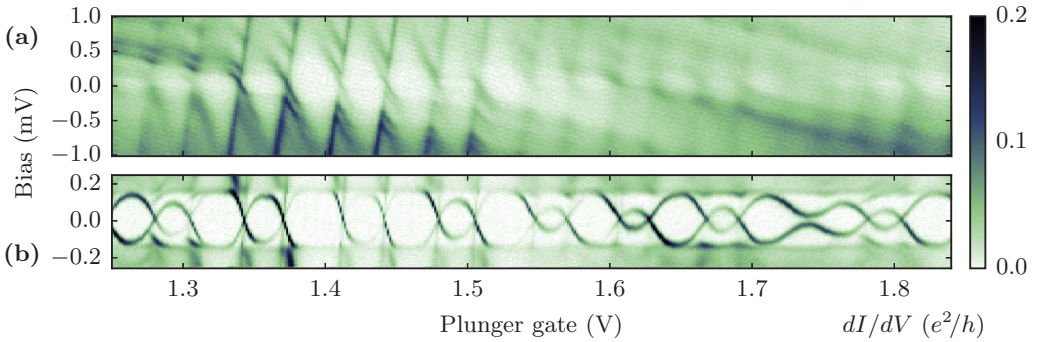

FIG. 3. Differential conductance at 35 mK with and without an externally applied 150-mT in-plane field. The field drives the aluminium contact normal in (b). Regions that show heavily tunnel-broadened Coulomb diamonds also show subgap excitations far inside the gap when the Al contact is superconducting.

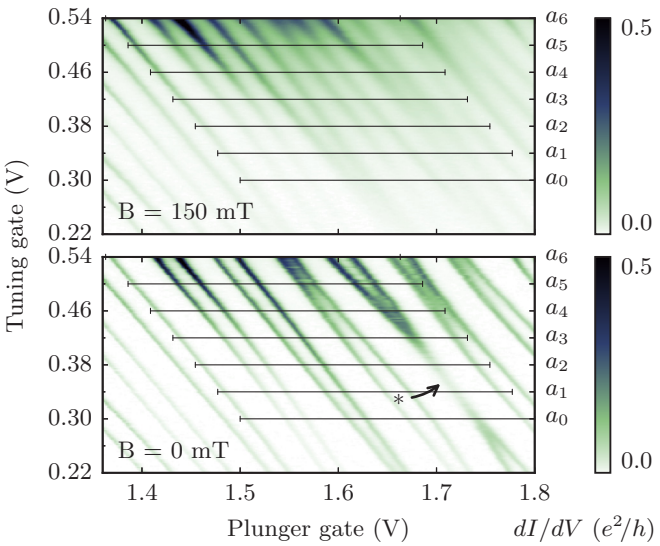

FIG. 4. Conductance at zero bias as a function of the tuning gate and the raw plunger gate potential, with and without a magnetic field driving the aluminium contact normal. The lines in these plots shows the cuts done by a_0–a_6 of Fig. 5. For certain configurations of the tuning gate, the ground state remains a singlet as a dot level is brought past the Fermi level with the plunger gate, and this is evident at the *.

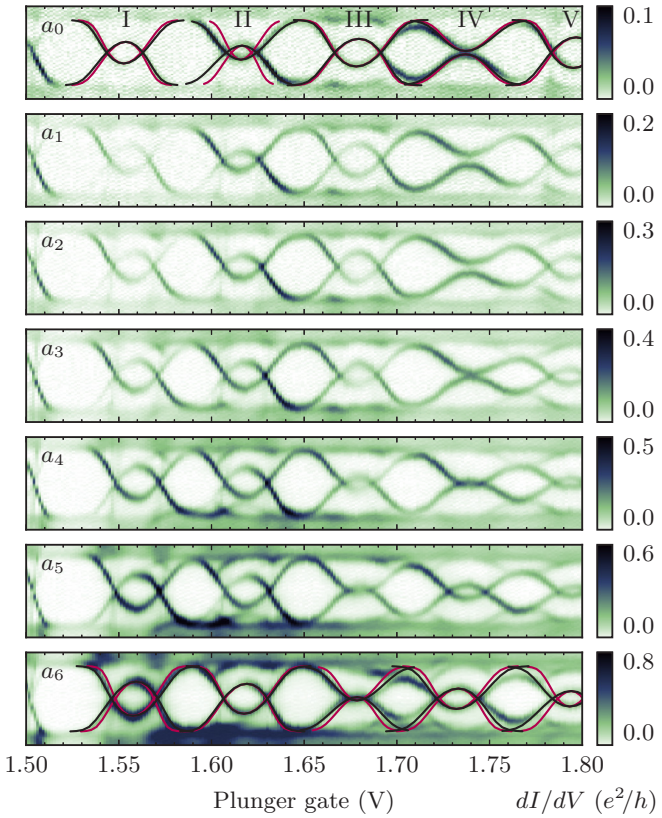

FIG. 5. Bias spectroscopy of the subgap states for different gate configurations. In every plot, the y axis is the potential of the superconducting lead relative to the normal lead and ranges from -0.2 to 0.2 mV. Note the different dI/dV scales. In the plot a_n, the tuning gate is set to $(300 + 40n)$ mV. We adjust for cross capacitance as described in the text. Example NRG fits are overlaid plots a_0 and a_6. The red curves are made using method 1 and the black curves are made using method 2; see text for details.

gate capacitance C_P, and the coupling strengths Γ_S and Γ_N. We will find quantitative estimates for all these parameters.

Specifically, we find U from the height of the corresponding Coulomb diamond in Fig. 3(a), and we find V_0 by looking at Fig. 5. We initially assume Γ_N is weak, in which case it has little effect on level positions and does not drive the NW-S system out of equilibrium, and we find C_P and Γ_S using one of two methods both involving a fit based on the NRG method: for method 1, we find C_P from the normal-state data in Fig. 4 and use Γ_S as a fitting parameter to fit the observed level positions. For method 2, we use both C_P and Γ_S as fitting parameters. Fits to two of the datasets are shown in Fig. 5 for both methods; the rest are included in the Supplemental Material [48].

Generally both methods reproduce the gate dependence of the subgap state excitations well. The most significant divergence is around $V_P' = 1.70$ V and $V_P' = 1.76$ V, where additional excitation lines are present inside the gap. The presence of these lines suggest that the levels are not independent in this region.

Having found the values of Γ_S at each level crossing from our NRG fits, we extract Γ_N from the conductance at each Coulomb peak when the superconductor is driven normal by an external magnetic field, i.e., from the data in Fig. 4. Specifically

$$G_{\text{peak}} = \frac{e^2}{h}\frac{4\Gamma_S\Gamma_N}{(\Gamma_S+\Gamma_N)^2}, \tag{1}$$

where G_{peak} is the maximal conductance of the device at the Coulomb peak [49]. The values of Γ_N and Γ_S that we extract are shown in Fig. 6. Γ_N shows an exponential dependence on the tuning gate potential, as expected for an electron tunneling through a potential barrier. In contrast, Γ_S varied nonmonotonically and did not have a systematic dependence

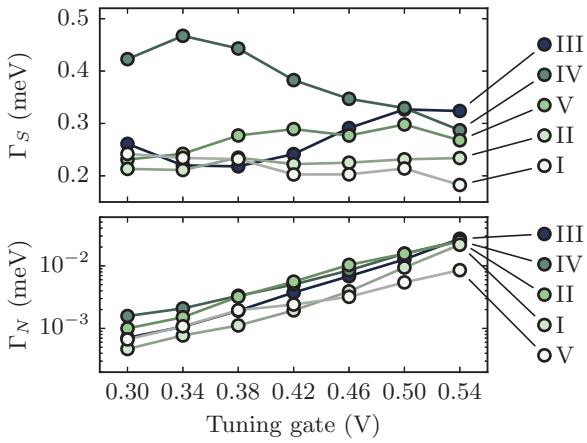

FIG. 6. Coupling strengths Γ_S and Γ_N of each level transition shown in Fig. 5. We extract Γ_S from our NRG fits, and use the conductance on resonance in the $B = 150$-mT data of Fig. 5 to find Γ_N. There is one trace in the plot for each level transition, and the roman numerals refer back to the labels in Fig. 5.

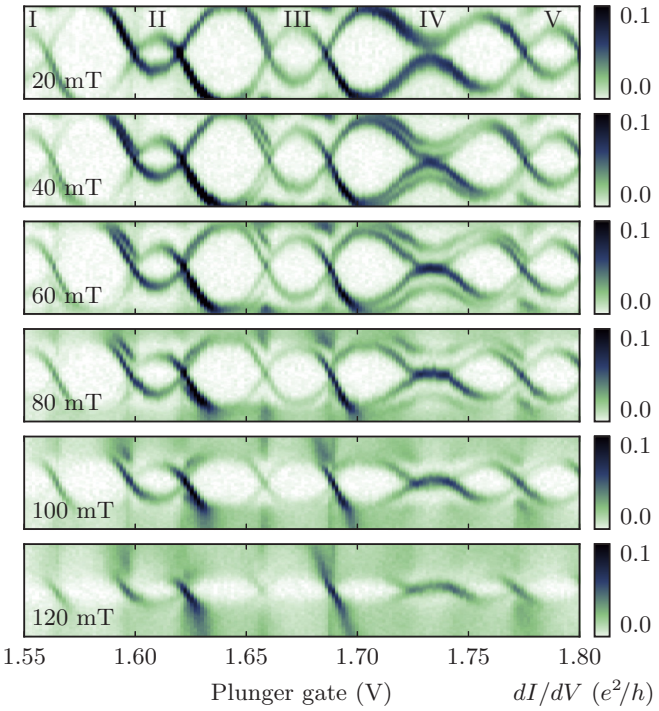

FIG. 7. Evolution of the subgap states as the gap closes upon the application of an external field in plane with the substrate perpendicular to the nanowire. The tuning gate is set to $V_T = 0.34$ V in all these plots, and the bias range is ± 125 μV. The roman numerals on odd charge states refer back to the labels in Fig. 5.

on gate. Therefore, we attribute the variations we do see in Γ_S to mesoscopic fluctuations caused by perturbations of the dot wave functions, rather than a changing potential barrier.

B. Results: Behavior at field

We now turn to the magnetic field dependence of the subgap states. Figure 7 shows what happens to the plot a_1 in Fig. 5 as a field is applied in the plane of the sample in a direction perpendicular to the nanowire. As the field increases, the doublet states Zeeman split, which is clear where the ground state is a singlet. When the ground state is a doublet, only one excitation is possible from the ground state, and only one peak is seen in transport [21]. When analyzing our data, we will augment the Anderson model Hamiltonian of the dot from the introduction with a Zeeman term of the form

$$H_Z = g\mu_B B \cdot S, \tag{2}$$

where g is the g factor of the level, μ_B is the Bohr magneton, B is the strength of the magnetic field, and S is the spin of the dot; note that we always align the z axis of the spin basis with the magnetic field. In our quantum dot, the effective g factor varies significantly between levels [50], and even within a single level. For instance, in the charge state labeled II in Fig. 7, the splitting of the excitations line left of center (near more negative V_P) is very different from the splitting right of center.

At the charge state labeled IV in Fig. 5 we are able to induce a quantum phase transition by a applying a magnetic field, so we focus on this level crossing. Figure 8 shows the dependence of transport at the center of the crossing both as the field magnitude is increased and as the field is rotated. As

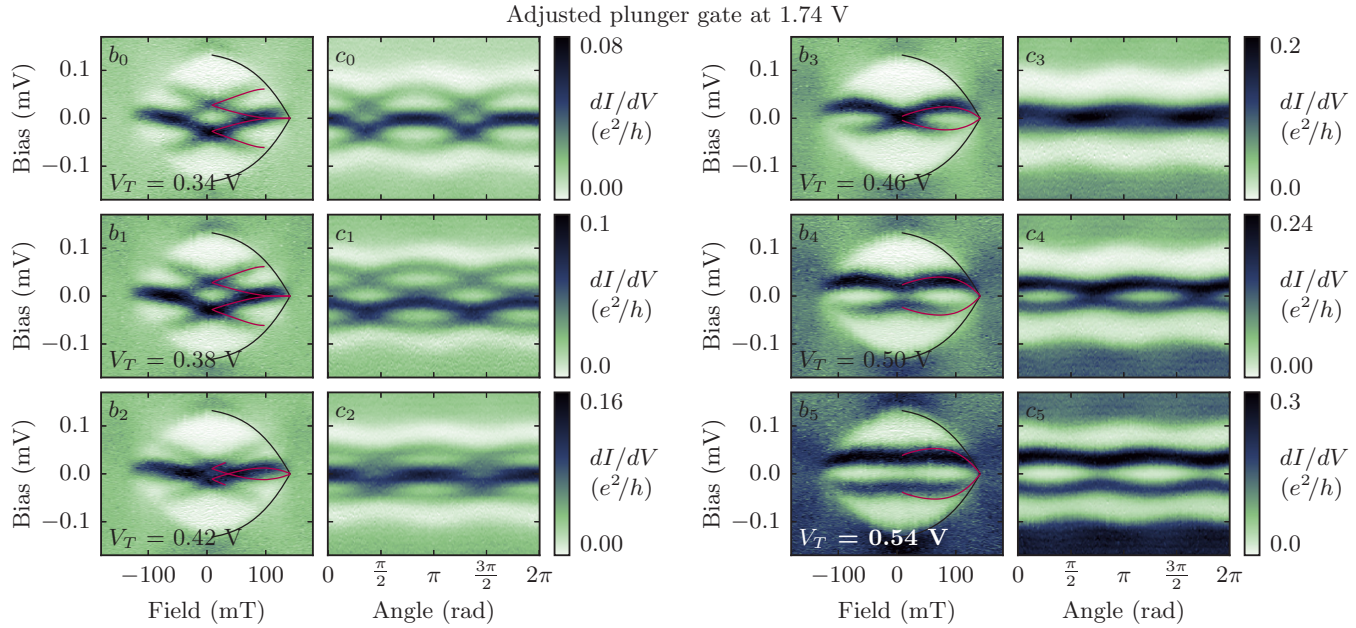

FIG. 8. Magnetic field dependence of subgap transport in the center of a level transition for different values of the tuning gate potential. In the data sets b_0 through b_5 the field was applied in the plane of the sample perpendicular to the nanowire, and in the data sets c_0 through c_5 the field was held at 60 mT and rotated in the plane of the sample with a direction of 0 radians being perpendicular to the wire. The data has been corrected for a drifting zero bias across the device as detailed in the Supplemental Material. The plots also show data from an NRG simulation, specifically the allowed excitations from the ground states of the system (red lines). The black lines show a phenomenological model of the gap closing used as an input to the simulation. Additional input to the simulation includes the Γ_S values from Fig. 6 and a g factor found by fitting the plot c_1 at 0 radians.

in our other dataset, we again note the absence of a transition from the excited member of the doublet to the singlet, which is what causes the peaks in Fig. 8 for $V_T > 0.42$ V to only move in one direction instead of splitting.

As is apparent in the plots c_0–c_5 of Fig. 8, the g factor of our system shows a high degree of anisotropy. This is a common property of quantum dots in InAs nanowires [50,51] and was also addressed by Lee *et al.* for Yu-Shiba-Rusinov (YSR) states [21].

In the bias vs field strength plots of Fig. 8, specifically plots b_0, b_1, and b_2, we note that the excitation of the doublet that moves down in energy has an apparent tendency to stick to zero bias. This effect has been observed before and can be understood in terms of a level repulsion from the gap states as the gap closes, pinning the excitations near zero energy [21]. We estimate the level positions from the data plotted in c_1 of Fig. 8, and fit the g factor at angles of 0, $0.9\,\pi$, and 1.4π rad using our NRG model. The latter two angles correspond to minimal and maximal Zeeman splitting; note that the splitting at 0.9π rad is hard to estimate precisely. For these angles, we find g factors of approximately 22, 8, and 23 respectively.

We use the g factor at 0 rad, along with the values of Γ_S found for each tuning gate value earlier, to simulate how the states split with applied field, i.e., to recreate the level positions seen in the plots b_0–b_5. The resulting level transitions are plotted in the figure and show good agreement with the data. We plot excitations from the ground state only, but in the plot b_2, transport is also possible from the doublet state, presumably because the doublet is thermally excited.

III. CONCLUSION

The device presented in this paper had two features that complement each other: Transparent contacts and well coupled bottom gates with a large admissible voltage range. This made it feasible to make completely gate defined contact barriers in the device, and tune coupling parameters over a large range while keeping mostly single-dot behavior. In combination with well resolved subgap states, the device provided an excellent platform to study the dependence of Yu-Shiba-Rusinov states to Γ_S tuning and to magnetic fields. Future studies may involve testing the recent theoretical predictions that the singlet-doublet phase diagram is modified by the normal-metal coupling [39].

For the data presented in this paper, we used a gate between the quantum dot and the normal contact to tune our device. This had a large effect on Γ_N which in turn has only a small effect on level positions. On the other hand, mesoscopic fluctuations of Γ_S (on the other side of the device) caused by this tuning has a large and, *a priori*, unpredictable effect on Γ_S. Effects like this can appear in gated quantum dot devices, whether it involves a superconducting contact or not, but this device is an interesting example as the two contact barriers influence transport in very dissimilar ways.

Modeling the device using the proximitized Anderson model by means of the NRG method yielded excitation energies in good agreement with our data, and the coupling parameters extracted from these fits follow the potentials of the bottom gates in a physically reasonable way. The behavior under magnetic field is entirely consistent with a simple Zeeman splitting in combination with the gap closing. This behavior has been described before [21]. However, here we model this scenario quantitatively using the NRG method starting from parameters determined at zero field, and show good agreement with observed data.

ACKNOWLEDGMENTS

We would like to thank R. Aguado and J. Paaske for helpful discussions and P. Krogstrup, C. B. Sørensen, and E. Johnson for experimental contributions. Funding for this project was provided by the EU FP7 project SE2ND (Source of Entangled Electrons in Nano Devices), the Carlsberg Foundation, the Danish Research Council DFF-FNU, and the Danish National Research Foundation.

APPENDIX A: FABRICATION DETAILS

The bottom gates were fabricated on a Si substrate with 500-nm oxide, and are composed of 5 nm Ti and 12 nm Au. These gates have a center-to-center distance of 55 nm. The gates are covered with 24 nm HfO_2 deposited by atomic layer depositioning. This HfO_2 is deposited in three 8-nm layers of successively smaller extent to avoid *fencing*, where the oxide does not break off cleanly where it meets resist walls and instead protrudes off the surface after lift-off.

70-nm-diameter InAs nanowires were deposited from a suspension in isopropanol. In the evaporation chamber, immediately prior to metalization of each contact, argon ion milling was used to remove the native oxide from the nanowire. The Au contact uses a 10-nm Ti sticking layer, and the Al contact uses a 5-nm Ti sticking layer. Compared to the data shown in this paper, the device is significantly more conductive when a higher potential is applied to the bottom gates, suggesting that the tunnel barriers seen in the data are gate defined as opposed to contact defined.

Tuning the potentials of the gates allows the device to be operated in different regimes; in this paper we focus on single dot behavior by forming a central potential dip (see Fig. 9). We note that bottom gates under a contact, for instance the second bottom gate from the right in Fig. 2, generally do not show any significant effect on transport through the device. This suggest that the gates are strongly screened, or that the contacts—by diverting current out of the wire already very near the edge of the contact—make it a moot point whether the sections of nanowire above these gates are depleted or not.

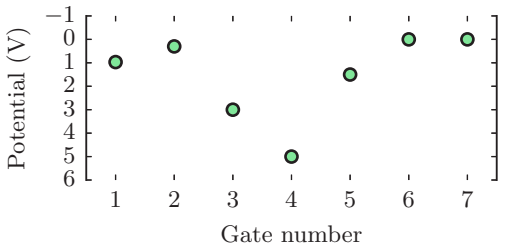

FIG. 9. Electric potentials applied to each relevant bottom gate. The gates are numbered starting from the gold side of the device (left side in Fig. 2). Gate no. 2 we call the tuning gate and gate no. 5, which is more strongly coupled to the energy levels of the dot, we call the plunger gate.

The device investigated in this paper forms part of a larger two-sided device. To avoid complications from the other side of the device, this part of the nanowire was electrostatically depleted during measurements.

APPENDIX B: MODEL DETAILS

For the discussions in the paper and in our models, we use the following Hamiltonian:

$$H = H_d + H_S + H_{tS} + H_{tN}, \tag{B1}$$

with each part given below. The quantum dot has the Hamiltonian

$$H_d = \sum_\sigma \epsilon_\sigma c_\sigma^\dagger c_\sigma + \frac{U}{2}\left(\sum_\sigma c_\sigma^\dagger c_\sigma - 1\right)^2, \tag{B2}$$

where $c_\sigma^\dagger$ creates an electron with spin σ on the dot, U is the charging energy of the dot, and ϵ is the single-particle energy of the dot. The dot is coupled to the two leads by

$$H_{tS} = \sum_{k\sigma} t_S c_\sigma^\dagger c_{k\sigma} + HC, \tag{B3}$$

$$H_{tN} = \sum_{k\sigma} t_N c_\sigma^\dagger f_{k\sigma} + HC, \tag{B4}$$

where $c_{k\sigma}^\dagger$ creates an ordinary fermion in the superconducting lead with momentum k and spin σ, $f_{k\sigma}^\dagger$ creates a fermion in the normal lead, and the t's are tunneling coefficients assumed spin and momentum independent. The Hamiltonian of the superconductor is

$$H_S = \sum_{k\sigma} \xi_{k\sigma} c_{k\sigma} c_{k\sigma}^\dagger + \sum_k (\Delta c_{k\uparrow} c_{-k\downarrow} + \Delta c_{-k\downarrow}^\dagger c_{k\uparrow}^\dagger), \tag{B5}$$

where Δ is the order parameter of the superconductor which we assume is real.

For our NRG simulations, we assume that t_N and the temperature of the system are negligible, we discretize the leads logarithmically using a discretization factor Δ of 2.5, and map the system to a chain of fermions starting with the quantum dot. We add sites of the chain one at a time and at each step retain the lower 160 eigenstates. The subgap excitation energies converge quickly [43], so we only extend the chain to 25 sites. To simulate the gap closing with applied field, we created, by hand, a table of gap size as a function of applied field based on the data in Fig. 8.

When calculating the peak conductance with the superconductor driven normal, in Eq. (1), we assume $k_B T \ll \Gamma_S + \Gamma_N$ consistent with our findings, and use a result from the Supplemental Material of Ref. [49].

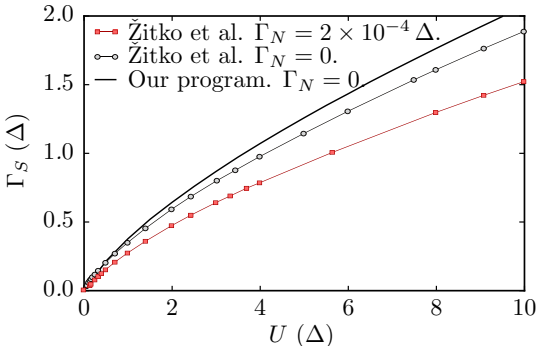

FIG. 10. This figure compares output from our NRG program to Fig. 1 in Ref. [39].

APPENDIX C: EVALUATING THE NRG PROGRAM

Since we are not exploiting symmetries in our NRG program, we cannot keep as many states as others do in the calculations. Therefore we compared the output of our program to a plot in Žitko *et al.* [39] showing the quantum phase transition in a proximitized dot (see Fig. 10). Žitko *et al.* also include simulations for a small coupling to the normal lead, which we reproduce in Fig. 10 to show that the error made by using our program is small compared to the error made by not considering finite Γ_N. Note that our definition of Γ_S differs from the one used in Žitko *et al.* by a factor of 2, so we scaled ours for this plot.

[1] S. De Franceschi, L. Kouwenhoven, C. Schönenberger, and W. Wernsdorfer, Nat. Nanotechnol. **5**, 703 (2010).
[2] J. D. Sau and S. D. Sarma, Nat. Commun. **3**, 964 (2012).
[3] M. Leijnse and K. Flensberg, Phys. Rev. B **86**, 134528 (2012).
[4] K. Flensberg, Phys. Rev. Lett. **106**, 090503 (2011).
[5] M. Leijnse and K. Flensberg, Phys. Rev. Lett. **107**, 210502 (2011).
[6] J. Alicea, Y. Oreg, G. Refael, F. von Oppen, and M. P. A. Fisher, Nat. Phys. **7**, 412 (2011).
[7] M. Leijnse and K. Flensberg, Phys. Rev. B **84**, 140501 (2011).
[8] Y. Cao, P. Wang, G. Xiong, M. Gong, and X.-Q. Li, Phys. Rev. B **86**, 115311 (2012).
[9] D. E. Liu and H. U. Baranger, Phys. Rev. B **84**, 201308 (2011).
[10] Y. Oreg, G. Refael, and F. von Oppen, Phys. Rev. Lett. **105**, 177002 (2010).
[11] J. D. Sau, R. M. Lutchyn, S. Tewari, and S. Das Sarma, Phys. Rev. Lett. **104**, 040502 (2010).
[12] P. Recher, E. V. Sukhorukov, and D. Loss, Phys. Rev. B **63**, 165314 (2001).
[13] L. Hofstetter, S. Csonka, J. Nygård, and C. Schönenberger, Nature (London) **461**, 960 (2009).
[14] L. G. Herrmann, F. Portier, P. Roche, A. L. Yeyati, T. Kontos, and C. Strunk, Phys. Rev. Lett. **104**, 026801 (2010).
[15] G. Kiršanskas, M. Goldstein, K. Flensberg, L. I. Glazman, and J. Paaske, Phys. Rev. B **92**, 235422 (2015).
[16] L. Yu, Acta Phys. Sin. **21**, 75 (1965).
[17] H. Shiba, Prog. Theor. Phys. **40**, 435 (1968).
[18] A. I. Rusinov, Sov. JETP Lett. **9**, 85 (1969).
[19] A. Yazdani, B. A. Jones, C. P. Lutz, M. F. Crommie, and D. M. Eigler, Science **275**, 1767 (1997).

[20] K. J. Franke, G. Schulze, and J. I. Pascual, Science **332**, 940 (2011).
[21] E. J. H. Lee, X. Jiang, M. Houzet, R. Aguado, C. M. Lieber, and S. De Franceschi, Nat. Nanotechnol. **9**, 79 (2014).
[22] K. Grove-Rasmussen, H. I. Jørgensen, B. M. Andersen, J. Paaske, T. S. Jespersen, J. Nygård, K. Flensberg, and P. E. Lindelof, Phys. Rev. B **79**, 134518 (2009).
[23] J.-D. Pillet, C. H. L. Quay, P. Morfin, C. Bena, A. L. Yeyati, and P. Joyez, Nat. Phys. **6**, 965 (2010).
[24] R. S. Deacon, Y. Tanaka, A. Oiwa, R. Sakano, K. Yoshida, K. Shibata, K. Hirakawa, and S. Tarucha, Phys. Rev. B **81**, 121308 (2010).
[25] T. Dirks, T. L. Hughes, S. Lal, B. Uchoa, Y.-F. Chen, C. Chialvo, P. M. Goldbart, and N. Mason, Nat. Phys. **7**, 386 (2011).
[26] R. S. Deacon, Y. Tanaka, A. Oiwa, R. Sakano, K. Yoshida, K. Shibata, K. Hirakawa, and S. Tarucha, Phys. Rev. Lett. **104**, 076805 (2010).
[27] W. Chang, V. E. Manucharyan, T. S. Jespersen, J. Nygård, and C. M. Marcus, Phys. Rev. Lett. **110**, 217005 (2013).
[28] B.-K. Kim, Y.-H. Ahn, J.-J. Kim, M.-S. Choi, M.-H. Bae, K. Kang, J. S. Lim, R. López, and N. Kim, Phys. Rev. Lett. **110**, 076803 (2013).
[29] A. Kumar, M. Gaim, D. Steininger, A. Levy Yeyati, A. Martín-Rodero, A. K. Hüttel, and C. Strunk, Phys. Rev. B **89**, 075428 (2014).
[30] J. Schindele, A. Baumgartner, R. Maurand, M. Weiss, and C. Schönenberger, Phys. Rev. B **89**, 045422 (2014).
[31] E. J. H. Lee, X. Jiang, R. Aguado, G. Katsaros, C. M. Lieber, and S. De Franceschi, Phys. Rev. Lett. **109**, 186802 (2012).
[32] J.-D. Pillet, P. Joyez, R. Žitko, and M. F. Goffman, Phys. Rev. B **88**, 045101 (2013).
[33] R. Delagrange, R. Weil, A. Kasumov, M. Ferrier, H. Bouchiat, and R. Deblock, Phys. Rev. B **93**, 195437 (2016).
[34] K. Wilson, Rev. Mod. Phys. **47**, 773 (1975).
[35] R. Bulla, T. Costi, and T. Pruschke, Rev. Mod. Phys. **80**, 395 (2008).
[36] V. Mourik, K. Zuo, S. M. Frolov, S. R. Plissard, E. P. A. M. Bakkers, and L. P. Kouwenhoven, Science **336**, 1003 (2012).
[37] A. Das, Y. Ronen, Y. Most, Y. Oreg, M. Heiblum, and H. Shtrikman, Nat. Phys. **8**, 887 (2012).
[38] S. M. Albrecht, A. P. Higginbotham, M. Madsen, F. Kuemmeth, T. S. Jespersen, J. Nygård, P. Krogstrup, and C. M. Marcus, Nature (London) **531**, 206 (2016).
[39] R. Žitko, J. S. Lim, R. López, and R. Aguado, Phys. Rev. B **91**, 045441 (2015).
[40] T. Meng, S. Florens, and P. Simon, Phys. Rev. B **79**, 224521 (2009).
[41] M. Tinkham, *Introduction to Superconductivity*, 2nd ed. (Dover, New York, 2004).
[42] S. Sachdev, in *Handbook of Magnetism and Advanced Magnetic Materials* (John Wiley & Sons, Hoboken, NJ, 2007).
[43] K. Satori, H. Shiba, O. Sakai, and Y. Shimizu, J. Phys. Soc. Jpn. **61**, 3239 (1992).
[44] O. Sakai, Y. Shimizu, H. Shiba, and K. Satori, J. Phys. Soc. Jpn. **62**, 3181 (1993).
[45] T. Yoshioka and Y. Ohashi, J. Phys. Soc. Jpn. **69**, 1812 (2000).
[46] Y. Tanaka, N. Kawakami, and A. Oguri, J. Phys. Soc. Jpn. **76**, 074701 (2007).
[47] A. Jellinggaard (unpublished).
[48] See Supplemental Material at http://link.aps.org/supplemental/10.1103/PhysRevB.94.064520 for additional fits and details on data treatment.
[49] H. I. Jørgensen, T. Novotný, K. Grove-Rasmussen, K. Flensberg, and P. E. Lindelof, Nano Lett. **7**, 2441 (2007).
[50] S. Csonka, L. Hofstetter, F. Freitag, S. Oberholzer, C. Schönenberger, T. S. Jespersen, M. Aagesen, and J. Nygård, Nano Lett. **8**, 3932 (2008).
[51] M. D. Schroer, K. D. Petersson, M. Jung, and J. R. Petta, Phys. Rev. Lett. **107**, 176811 (2011).